Non-collinear antiferromagnetism in FeCrAs

Swainson, Ian P.; Wu, Wenlong; McCollam, Alix; Julian, Stephen R.

Publisher's version / Version de l'éditeur:
https://doi.org/10.1139/P09-050
Canadian Journal of Physics, 88, 10, pp. 701-706, 2010-04-30

Non-collinear antiferromagnetism in FeCrAs [1]

Ian P. Swainson, Wenlong Wu, Alix McCollam, and Stephen R. Julian

Abstract: FeCrAs undergoes a magnetic ordering transition at $T_N \simeq 125$ K. The magnetic structure of FeCrAs, which crystallizes in space group $P\bar{6}2m$ and is isostructural to Fe_2P, was determined by constant wavelength neutron powder diffraction. A single basis function was found to describe the intensity distribution in the magnetic satellite reflections, which are associated with propagation vector $\boldsymbol{k}$ = (1/3, 1/3, 0), representing a *K*-point zone-boundary ordering. The magnetic intensity could be modelled by moments from Cr only, which lie on the 3*g*-sites, in pyramidal coordination by As, whereas the moments on Fe, in tetrahedral coordination on the 3*f*-sites, were found to be so small as to be zero within error. This agrees with previous Mössbauer spectroscopy measurements on this compound. The magnetic structure is characterized by non-collinear antiferromagnetic order of the moments, all of which lie in the hexagonal plane. This does not appear to have been observed in other monopnictides with Fe_2P structure but is consistent with geometric frustration of antiferromagnetic interactions.

PACS Nos: 72.80.Ga, 75.25.+z, 75.50.Ee, 75.50.Pp, 61.05.F–

Résumé : FeCrAs subit une transition magnétique à $T_N \simeq 125$ K. La structure magnétique de FeCrAs, qui cristallise dans le groupe spatial $P\bar{6}2m$ et est isostructural à Fe_2P, a été déterminée par diffraction de faisceaux de neutrons ayant une longueur d'onde constante. Une seule fonction de base suffit pour décrire la répartition des intensités des réflexions magnétiques auxilliaires, qui sont associées au vecteur de propagation $\boldsymbol{k}$ = (1/3, 1/3, 0), le *K*-point au bord de la zone de Brillouin. Les intensités magnétiques peuvent être modélisées par les moments des atomes de Cr seulement, qui se trouvent sur les sites 3*g*, en coordinence pyramidale à base carrée avec les atomes de As, tandis que les tailles des moments des atomes de Fe, en coordinence tétraédrique sur les sites 3*f*, ont été jugés si petites qu'elles sont zéro dans la marge d'erreur. Cela concorde avec les précédentes mesures par spectroscopie Mössbauer sur ce composé. La structure magnétique est caractérisée par un ordre des moments antiferromagnétique et non-collinéaire, tous liés dans le plan hexagonal. Cela ne semble pas avoir été observé dans d'autres monopnictides de structure Fe_2P, mais est compatible avec une frustration géométrique des interactions antiferromagnétiques.

[Traduit par la Rédaction]

1. Introduction

FeCrAs is a member of a family of monopnictides of 3*d*-metals. The crystal chemistry of this family with members of the 3*d*, 4*d*, and 5*d* transition elements has been reviewed by Fruchart [1]. There are three dominant crystal structure types for this family: Fe_2As (tetragonal), Co_2P (orthorhombic), and Fe_2P (hexagonal). FeCrAs crystallizes in this latter form [1, 2]. All three crystal structure types consist of two distinct types of polyhedra of pnictides surrounding the transition metal atoms: tetrahedra and square-based pyramids [1]. The usual rule is that the more electropositive transition element sits in the pyramidal site [1]. The difference lies in the manner in which the two units are joined together. In the Fe_2P structure type, which is characterized by the $P\bar{6}2m$ space group, the square-based pyramidal sites lie on the Wyckoff 3*g*-sites, and the tetrahedral sites lie on the 3*f*-sites, both having site symmetry m2m. The tetrahedra form trimers that share one common edge running along *c* and are corner-connected to neighbouring trimers in the hexagonal plane and to trimers above and below them. The pyramids share all the edges of their square bases with neighbouring pyramids, and their apices are corner-shared between them (Fig. 1). An alternate description, useful from the point of magnetic exchange, is in terms of the metal sublattices: in such a description, the Fe atoms lie in distinct trimers, while Cr atoms lie in a distorted kagome lattice, both of these units lying in the hexagonal plane (Fig. 1). The metal–metal distances in these pnictide compounds are closer to those seen in metals than those seen in their corresponding oxides [1].

Ishida et al. calculated energy band structures for various transition-metal pnictides and showed that for FeCrAs, in particular, the energy difference between paramagnetic, ferromagnetic, and antiferromagnetic states was very small [3]; they predicted that FeCrAs should be a ferromagnet. Mössbauer measurements on this compound found no evidence for ferromagnetic order, as the moment on Fe was estimated

Received 10 March 2009. Accepted 19 April 2009. Published on the NRC Research Press Web site at cjp.nrc.ca on 30 April 2010.

I.P. Swainson.[2] Canadian Neutron Beam Centre, National Research Council of Canada, Chalk River, ON K0J 1J0, Canada. **W. Wu, A. McCollam,**[3] **and S.R. Julian.** Department of Physics, University of Toronto, 60 St. George Street, Toronto, ON M5S 1A7, Canada.

[1]Special issue on Neutron Scattering in Canada.
[2]Corresponding author (e-mail: Ian.Swainson@nrc.gc.ca).
[3]Present address: High Field Magnet Laboratory, Institute for Molecules and Materials, Radboud University Nijmegen, Toernooiveld 7, 6525 ED, Nijmegen, Netherlands.

Fig. 1. Oblique view of the Fe_2P structure type shown with the metal atoms in polyhedral coordination by As (grey atoms), with light-coloured tetrahedra (green online) and dark square-based pyramidal (red online) sites. Isolated view down the *c*-axis of the Fe (green) and Cr (red) metal sublattices in their triangular and distorted kagome lattice, respectively. The metal–metal distances are given in Å.

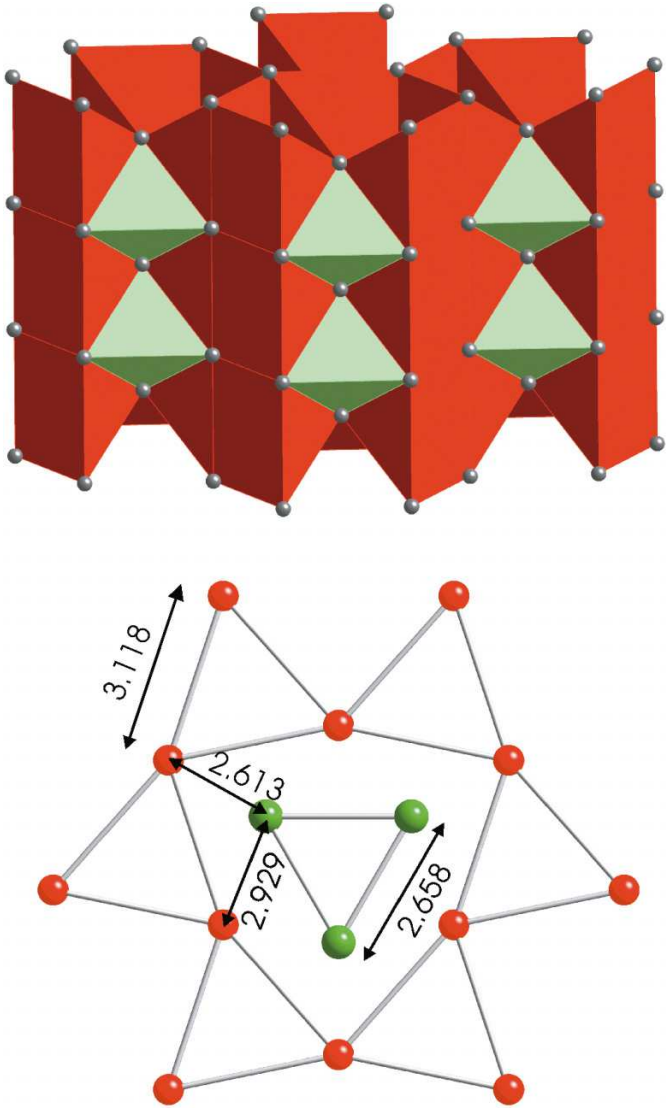

to be less than 0.1 ± 0.03 μB [4]. One possibility was that FeCrAs was a paramagnet down to 4.2 K [4]; another was that only Cr orders magnetically.

A recent investigation of the magnetic properties of single crystals of FeCrAs has shown several unusual features, including strong nonmetallic behaviour of the in-plane and out-of-plane resistivities with negative $d\rho/dT$ up to high temperatures, while at low temperatures both resistivities have strongly nonmetallic, non-Fermi-liquid behaviour. The magnetic susceptibility was found to be relatively flat as a function of temperature, with a weak peak at 125 K, and no Curie–Weiss behaviour was found [5]. This study also noted the unusually low moment on the Fe atom, and that several of these features are reminiscent of the new class of iron pnictide superconductors.

Several similar studies have been performed in the past on Fe_2P, Co_2P, and Fe_2As structure types. Many of these have relatively high magnetic ordering temperatures. Magnetic structures of several metal monopnictides with Fe_2P structure have been studied, including CrNiAs [6, 7], Fe_2P [8, 9], and Mn_2P [10], but so far there have been no reports of the magnetic structure of FeCrAs. Because of the unusual magnetic properties of this compound [5], it was decided to use neutron powder diffraction to investigate the ordered magnetic ground state.

2. Experimental

Single crystals of FeCrAs were grown by melting high purity Fe, Cr, and As in stoichiometric ratio following the recipe given by Katsuraki and Achiwa [11]. Several batches of crystals were grown and annealed at 900 °C in vacuum for 5–10 days. The single crystals were used for susceptibility and resistivity measurements that have been published elsewhere [5]. Some of these were ground to powder for neutron diffraction measurements that were performed on the C2 neutron powder diffractometer, located at the NRU reactor, Chalk River, Ontario. C2 consists of an 800-wire BF_3 detector, floating via high pressure air pads on an epoxy dancefloor. Measurements were performed at $\lambda = 2.37$ Å using a flat Si 311 monochromator. Although there is no $\lambda/2$ coming directly from such a monochromator, a Panasonic pyrolitic "Super Graphite" filter was used to clean up the beam, which results in better signal-to-noise in the measured diffraction pattern. Approximately one cubic centimetre of powdered sample was placed inside a thin-walled vanadium can of radius 5 mm. The measurements were performed with the can mounted inside in a pumped-^{4}He, ILL-style "Orange" cryostat. Temperatures were monitored and controlled using individually calibrated Cernox resistive temperature devices and a PC-based controller with a home-written control program. The lowest temperature reached was 2.8 K.

3. Data analysis and methods

The nuclear and magnetic structures were modelled as separate phases in the program Fullprof 2006 [12]; the magnetic phase was related to the nuclear phase using the propagation vector method, and the refinements of the possible magnetic moment orientations were constrained by using the basis vector approach; refining the coefficients of these basis vectors simultaneously allows for linear admixtures of the symmetry-allowed states, if required, and for varying the size of the magnetic moments. For the refinements of the nuclear phase, the default 2200 m/s thermal scattering lengths, *b*, of the elements, as given by Sears [13, 14] and encoded in Fullprof, were used [12, 15]. The magnetic form factors used for the Fe^{3+} and Cr^{3+} sites were the series approximation to $< j_0(\sin\theta)/\lambda >$ given by Brown [16], and encoded in Fullprof, as MFE3 and MCR3 [15]. The material is not a strong absorber, so no special correction was applied.

4. Refinement

As in the case of the neutron powder diffraction studies of CrNiAs, there is very high scattering contrast between Fe ($b = 9.45$ fm) and Cr ($b = 3.635$ fm) [13, 14], and this was sufficient to demonstrate that in FeCrAs, complete ordering

of Cr takes place in the square-based pyramidal 3g sites, and correspondingly, of Fe in the tetrahedral 3f sites. This agrees with the crystal chemical trends observations of Fruchart, who reported that the more electronegative element would be expected to occupy the tetrahedral site: Fe has 1.83 and Cr 1.66 on the Pauling scale of electronegativity [17, 18]. Here 3*f* and 3*g* denote both the site multiplicity and the Wyckoff site symbols for the space group P$\bar{6}$2m [1].

On cooling below T_N to 2.8 K, new satellite peaks appeared, demonstrating that both paramagnetism and the predictions of Ishida et al. [3] of simple ferromagnetism were impossible. This agreed with the susceptibility measurements on single crystals that showed non-Curie–Weiss behaviour and a peak at 125 K. We found that the propagation vector $\boldsymbol{k}$ = (1/3, 1/3, 0) was required to index the magnetic satellite peaks. This vector corresponds to a high-symmetry point on an edge of the Brillouin zone of a primitive hexagonal material (Fig. 2), labelled the *K*-point by Bradley and Cracknell [19].

Fig. 2. The Brillouin zone of a Primitive hexagonal lattice (after [19]), with high-symmetry points labelled, Γ = (0,0,0), M = (1/2,0,0), K = (1/3,1/3,0), L = (1/2,0,1/2), H = (1/3,1/3,1/2), and A = (0,0,1/2).

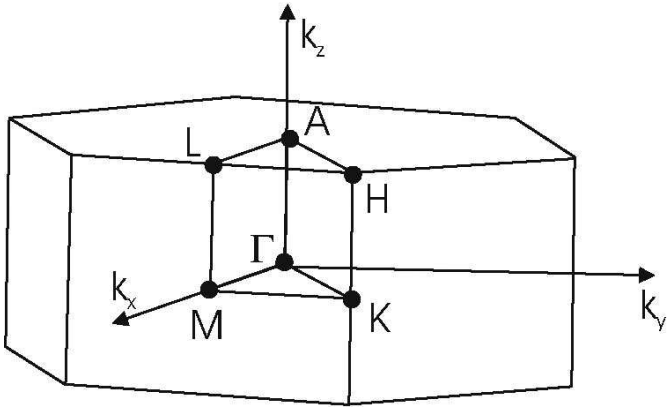

4.1. Representational analysis

Symmetry analysis was performed using the Sara*h* (version 7.1.3) [20]. Both the 3*g*-pyramidal and 3*f*-tetrahedral sites have the same point symmetry (m2m), and therefore the total magnetic representation for the 3*f* and 3*g* sites is the same:

$$\Gamma_{\mathrm{mag}} = \Gamma_2^1 + \Gamma_3^1 + \Gamma_4^1 + \Gamma_5^2 + \Gamma_6^2 \qquad (1)$$

where Γ_i^j is an irreducible representation, and the subscript labels, *i*, identify the representation according to the scheme of Kovalev [21], and the superscripts, *j*, define the dimensionality of the representation. Representational analysis shows that for both pyramidal and tetrahedal sites, the five irreducible representations describe nine basis vectors, Ψ_m, governing the allowed magnetic ordering schemes, with each one-dimensional representation having one, and Γ_5^2 and Γ_6^2 having two and four, respectively. The subscripts *m* of the basis vectors, Ψ_m, utilized by Sara*h* are allocated sequentially to the basis vectors of each Γ_i^j and have no special meaning. Both the basis vectors, Ψ_m, and the phase factors, exp $2\pi i\boldsymbol{k}\cdot\boldsymbol{t}$, are generally complex. Sara*h* transforms the basis vectors to real functions for refinement. At the surface of the Brillouin zone, the vector $\boldsymbol{k}$ is symmetrically equivalent to $-\boldsymbol{k}$; the propagation vector $-\boldsymbol{k}$ was included in the refinement, which also ensures that the phase factors are real. The refined moments $\boldsymbol{m}$ on the *l*th atom are related by the equation,

$$\boldsymbol{m}_l = 2\,\mathrm{Re}(\Psi_{m,l})\cos(2\pi\boldsymbol{k}\cdot\boldsymbol{t})$$

where $\boldsymbol{t}$ are translational operators in the unit cell.

Given that the Mössbauer evidence suggested that Fe did not order magnetically, the initial fits concentrated on fitting only the Cr moments, and all of the possible basis functions were tested by varying their associated coefficients in the Rietveld fit. Fits using moments on Cr alone proved quite successful at describing the magnetic intensity. A fit to a single basis function, $\Gamma_6^2\Psi_6$, proved sufficient to describe the observed magnetic reflections and was clearly superior to the other possibilities, with a magnetic reliability factor of R_{mag} of 19.8% (Table 1). All the moments are constrained to lie in the hexagonal plane by this basis vector. The difference in the quality of the magnetic fits by the different $\Gamma_i^j\Psi_m$ was quite marked: the next best candidate was $\Gamma_6^2\Psi_9$ with an R_{mag} of 35.9%, and the worst fit was to $\Gamma_2^1\Psi_1$ with an R_{mag} of 64.7%.

Given that there is only one apparent magnetic transition, if both sites ordered, it would be likely that the magnetic order on the two metal sublattices would be governed by the same irreducible representation. Tests were performed to see if a small magnetic moment could be found on the Fe atom, by performing refinements based on the four basis vectors of the Γ_6^2 irreducible representation and linear admixtures of these. None proved successful. For the refinements assuming $\Gamma_6^2\Psi_6$ as the ordering scheme on both Fe and Cr, a small coefficient of opposite sign to that on Cr was found on Fe in the refinements, but the error was always larger than the value of the coefficient. Also, while the refined coefficient of the moment on Cr showed a temperature dependence that followed that of the magnetic peaks, the small refined moments on Fe remained almost constant with temperature. For these reasons, we assume that the Fe moments are so small as to be not quantifiable from these data, in agreement with the previous Mössbauer data, which suggested a mean moment less than 0.1 ± 0.03 μB [4]. The final fit is shown in Fig. 3.

We note in passing that the Fe_2P structure type is commonly referred to as the ZrNiAl structure type for rare earth – transition metal intermetallic (RTX) compounds, and that almost 30% of these crystallize in this form [22]. In this structure type, the rare earth, R, occupies the pyramidal site, analogous to Cr in this compound. The problems associated with antiferromagnetic interactions and magnetic ordering for rare earth atoms in this distorted kagome lattice have been discussed and modelled in terms of classical spins; ordered structures with propagation vectors of $\boldsymbol{k}$ = (1/3, 1/3, 0) have been predicted [22], although they differ in detail from the one observed here, and seen in the compounds DyAgSi and HoAgSi [23], and DyAgGe and HoAgGe [24].

Table 1. Description of nuclear and magnetic structures.

Nuclear structure							
$P\bar{6}2m$							
a (Å)	c (Å)						
6.0675(7)	3.6570(5)						
Atom	Wyckoff site	x	y	z			
Cr	3g	0.564(4)	0	1/2			
Fe	3f	0.240(2)	0	0			
As	2c	1/3	2/3	0			
As	1b	0	0	1/2			
Magnetic structure							
Propagation vector description							
$\boldsymbol{k}$	1/3	1/3	0				
$c\Gamma_6^2\Psi_6$[a]	–0.685(40)						
Basis vector $\Gamma_6^2\Psi_6$ in terms of real and imaginary components of moments perpendicular to mirrors							
Atom[b]	Mag.[c]	m_a	m_b	m_c	im_a	im_b	im_c
x,0,1/2	4	4	0	0	0	0	0
0,x,1/2	2	0	–2	0	0	0	0
1-x,1-x,1/2	1	–1	–1	0	$\sqrt{3}$	$\sqrt{3}$	0
Shubnikov description[d]							
Am′m′2							
a (Å)	b (Å)	c (Å)					
3.657	10.509	18.203					
***R*-factors**							
R_{Bragg}	R_{F}	R_{Mag}					
10.9%	6.21%	19.8%					

[a] $c\Gamma_6^2\Psi_6$ is the coefficient of the magnetic basis vector $\Gamma_6^2\Psi_6$.

[b] The symmetry copies of Cr in $P\bar{6}2m$; $x = 0.564$.

[c] "Mag." $\times\ c\Gamma_6^2\Psi_6$ gives the moment in μB.

[d] The atom coordinates in the Shubnikov cell can be derived from the nuclear cell by the inverse transpose of the transformation matrix given in eq. (2).

Fig. 3. Plot of the fit to the nuclear and magnetic peaks of FeCrAs at 2.8 K. There were no discernible magnetic peaks above 60° 2θ. The upper tic marks correspond to peaks from the nuclear phase, and the lower tic marks correspond to those of the magnetic phase.

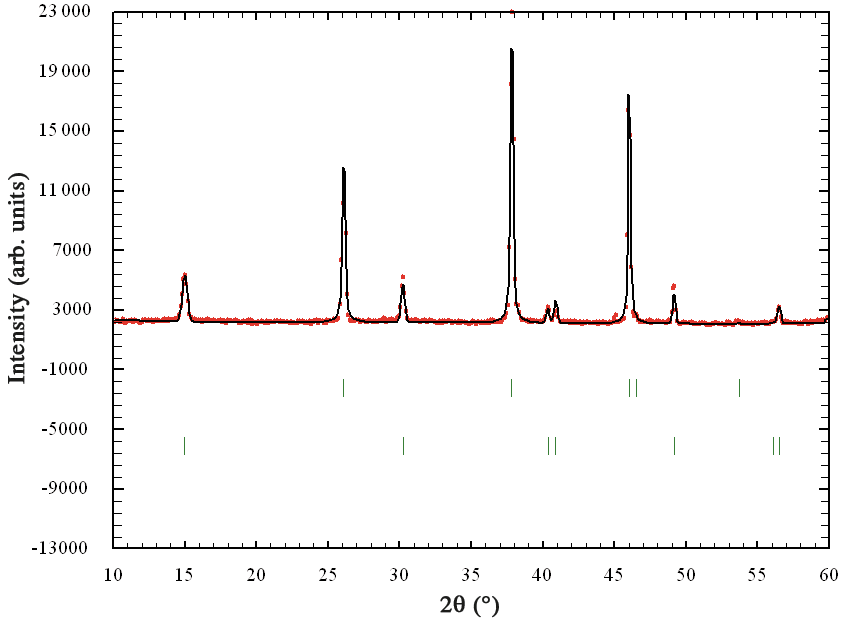

Table 2. Ordered moments on the two metal sites of various Fe_2P-structure monopnictides.

	Pyramidal 3*g*		Tetrahedral 3*f*				
	Moment (μB)		Moment (μB)		Order[a]	T_c or T_N (K)	Ref.
Fe_2P	Fe	2.22±0.01	Fe	0.59±0.02	F//*c*	217	7, 8
CrNiAs	Cr	1.25±0.05	Ni	0.15±0.03	F//*c*	182	6, 7
	Cr	2.27, 2.03	Ni	0.78, 0.36	AF//*a*	110	
					F//*c*		
Mn_2P	Mn[b]	0.84±0.03	Mn[b]	0.01±0.04	AF//*b*	103	10
MnFeAs	Fe	3.14±0.02	Mn	1.54±0.03	F//*c*	190	7

[a]F = Ferromagnetic, AF = Antiferromagnetic.
[b]Mean values.

Fig. 4. Top: View of the magnetic and nuclear cells and of the ordered moments on Cr, where +c goes down into the page. The moments are colour-coded (online) according to the size of the moment, to aid the eye. The nuclear cell is the smallest hexagonal cell. The $3 \times 3 \times 1$ supercell, corresponding to the propagation vector $\boldsymbol{k}$ = (1/3,1/3,0), is shown as a bold hexagonal cell. The alternate description in terms of the orthorhombic Shubnikov group Am′m′2 is also shown as a bold unit cell, with bold dots indicating lattice points. Bottom: View of the symmetry elements that lie in the Shubnikov cell, with double lines, solid and dashed, representing antiunitary planes of symmetry, antimirrors, and antiglides, respectively.

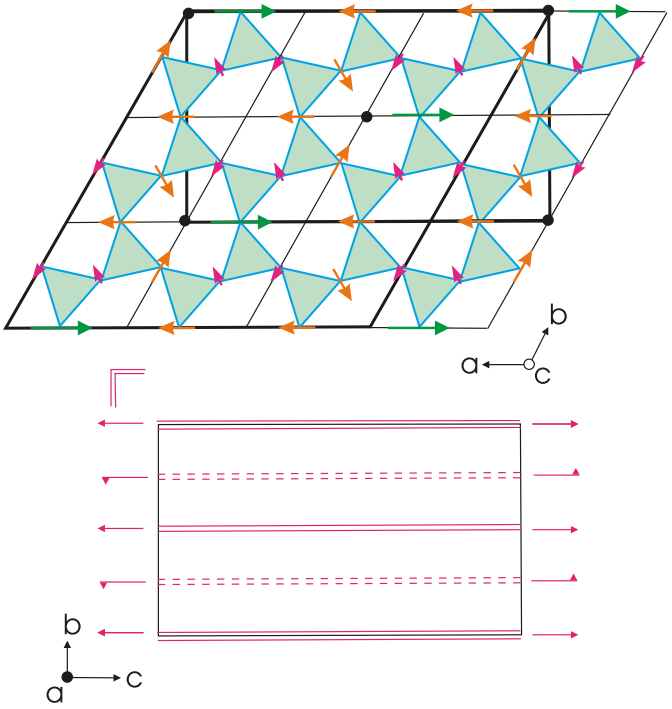

4.2. Colour group symmetry

As the propagation vector, lying along the Brillouin Zone edge, is a rational fraction of the nuclear unit cell, the magnetic order can be depicted as a commensurate $3 \times 3 \times 1$ supercell of the nuclear structure, as well as within the more restrictive terms of colour groups [25–27]. The results of the refinement of the magnetic structure are tabulated in Table 1, together with the definition of the basis vector $\Gamma_6^2\Psi_6$ describing the ordered ground state of the Cr moments; the magnetic moments on Cr are oriented along $< 1, 0, 0 >$, $< 0, \bar{1}, 0 >$, and $< \bar{1}, \bar{1}, 0 >$ directions. The basis function $\Gamma_6^2\Psi_6$ dictates that the moments on Cr are 1-, 2-, and 4-times multiples of the refined coefficient 0.685 μB; there are, respectively, 12, 12, and 3 of these different moments in the hexagonal supercell, so that the average moment on Cr is 1.22 μB, while the net moment per cell remains zero. This state is depicted pictorially in Fig. 4, where the nuclear cell, the $3 \times 3 \times 1$ hexagonal supercell corresponding to the refinement with the propagation vector model in Fullprof, and the Shubnikov cell are shown together.

The alternative orthorhombic description of the magnetic cell (Fig. 4) corresponding to the Shubnikov group Am′m′2 is related to the nuclear cell, with no change in origin, by

$$\begin{pmatrix} a \\ b \\ c \end{pmatrix}_{\mathrm{Am'm'2}} = \begin{pmatrix} 0 & 0 & 1 \\ 1 & 2 & 0 \\ -3 & 0 & 0 \end{pmatrix} \begin{pmatrix} a \\ b \\ c \end{pmatrix}_{\mathrm{P\bar{6}2m}} \quad (2)$$

The coordinates can be mapped from the hexagonal cell to the orthorhombic cell using the inverse transpose of the above matrix.

Table 2 gives a comparison to other ordered magnetic structures that are found in Fe_2P-type compounds. Both CrNiAs ($T < 110$ K) and Mn_2P are associated with antiferromagnetism, with moments parallel to the hexagonal axis, and can be described in another orthorhombic cell, related to the hexagonal cell by,

$$\begin{pmatrix} a \\ b \\ c \end{pmatrix} = \begin{pmatrix} 2 & 1 & 0 \\ 0 & 1 & 0 \\ 0 & 0 & 1 \end{pmatrix} \begin{pmatrix} a \\ b \\ c \end{pmatrix}_{\mathrm{P\bar{6}2m}} \quad (3)$$

Such ordering is likely governed by an *M*-point representation (Fig. 2), although CrNiAs has an additional incommensurate propagation vector along c^* [6, 7]. The pattern of having small moments on the tetrahedral sites does not just hold for Fe_2P structure types, but appears to hold in those cases of magnetic order that have been reported for both the Fe_2As-type (e.g., the high-pressure polymorph of MnFeAs [7]), and Co_2P-type structures (e.g., FeMnP [28], Cr_2As [29], and $(Co_{1-x}Mn_x)_2P$ [30]).

5. Conclusions

The non-collinear antiferromagnetism observed in FeCrAs appears to be unique among those spin structures that have been reported in the transition-metal compounds that crystal-

lize in the Fe_2P structure type. However, non-collinear antiferromagnetism has been observed in FeMnP, a Co_2P-type structure. Such ordering schemes can be expected from geometric frustration of systems with in-plane antiferromagnetic interactions. Since the energy differences between ferro-, antiferro-, and paramagnetism are typically low in such systems, and in the case of FeCrAs, in particular [3], the magnetic phase diagram in these systems is likely to be complex. The high ordering temperatures of these compounds would make a study of the pressure dependence of the spin structures in such compounds relatively simple.

Acknowledgments

SRJ gratefully acknowledges the support of the Canadian Institute for Advanced Research and the Natural Sciences and Engineering Research Council (NSERC). Access to the Canadian Neutron Beam Centre is supported by the NSERC Major Resources Support Program.

References

1. R. Fruchart. Ann. Chim. **7**, 563 (1982).
2. M.A. Nylund, M.M.A. Roger, J.P. Senateur, and R. Fruchart. J. Solid State Chem. **4**, 115 (1972). doi:10.1016/0022-4596(72)90139-9.
3. S. Ishida, T. Takaguchi, S. Fujii, and S. Asano. Physica B, **217**, 87 (1996). doi:10.1016/0921-4526(95)00538-2.
4. D.G. Rancourt. Ph.D. thesis, Toronto. 1983.
5. W. Wu, A. McCollam, I. Swainson, P.M.C. Rourke, D.G. Rancourt, and S.R. Julian. EPL, **85**, 17009 (2009). doi:10.1209/0295-5075/85/17009.
6. M. Bacmann, D. Fruchart, A. Koumina, and P. Wolfers. Mater. Sci. Forum, **443–444**, 379 (2004). doi:10.4028/www.scientific.net/MSF.443-444.379.
7. A. Koumina, M. Bacmann, D. Fruchart, M. Mesnaoui, and P. Wolfers. Moroccan J. Condens. Matter, **5**, 117 (2004).
8. A. Koumina, M. Bacmann, D. Fruchart, J.-L. Soubeyroux, P. Wolfers, J. Tobola, S. Kaprzyk, S. Niziol, M. Mesnaoui, and R. Zach. Ann. Chim. - Sci. Mat. **23**, 177 (1998). doi:10.1016/S0151-9107(98)80050-0.
9. D. Scheerlinck and E. Legrand. Solid State Commun. **25**, 181 (1978). doi:10.1016/0038-1098(78)91474-6.
10. M. Yessik. Philos. Mag. **17**, 623 (1968). doi:10.1080/14786436808217748.
11. H. Katsuraki and N. Achiwa. J. Phys. Soc. Jpn. **21**, 2238 (1966). doi:10.1143/JPSJ.21.2238.
12. J. Rodriguez-Carvajal. Physica B, **192**, 55 (1993). doi:10.1016/0921-4526(93)90108-I.
13. V.F. Sears. *In* International Tables for Crystallography. Vol. C, 444 (2006).
14. V.F. Sears. Neutron News, **3**, 29 (1992). doi:10.1080/10448639208218770.
15. FullProf Users' Guide. Available from http://www.ill.eu/sites/fullprof/downloads/-FullProfManual.zip.
16. P.J. Brown. *In* International Tables for Crystallography. Vol. C, 454 (2006).
17. L. Pauling. J. Am. Chem. Soc. **54**, 3570 (1932). doi:10.1021/ja01348a011.
18. A.L. Allred. J. Inorg. Nucl. Chem. **17**, 215 (1961). doi:10.1016/0022-1902(61)80142-5.
19. *In* Mathematical Theory of Symmetry in Solids. *Edited by* C.J. Bradley and A.P. Cracknell. Oxford University Press, Oxford, UK. 1972.
20. A.S. Wills. Physica B, **276–278**, 680 (2000). doi:10.1016/S0921-4526(99)01722-6.
21. O.V. Kovalev. Representations of the Crystallographic Space Groups. Gordon and Breach Science Publishers, Switzerland. 1993.
22. Ł. Gondek and A. Szytuła. J. Alloy. Comp. **442**, 111 (2007). doi:10.1016/j.jallcom.2006.07.136.
23. S. Baran, M. Hofmann, J. Leciejewicz, B. Penc, M. Ślaski, A. Szytuła, and A. Zygmunt. J. Magn. Magn. Mater. **222**, 277 (2000). doi:10.1016/S0304-8853(00)00565-5.
24. S. Baran, M. Hofmann, J. Leciejewicz, B. Penc, M. Ślaski, and A. Szytuła. J. Alloy. Comp. **281**, 92 (1998). doi:10.1016/S0925-8388(98)00721-X.
25. S.J. Joshua. *In* Symmetry principles and magnetic symmetry in solid state physics. Adam Hilger, Bristol, UK. 1991.
26. W. Opechowski and R. Guccione. *In* Magnetism. *Edited by* G.T. Rado and H. Suhl.Vol. 2A, Ch. 3, New York Academic Press, N.Y., USA. 1965.
27. A.V. Shubnikov, N.V. Belov, and W.T. Holse. Colored symmetry. Pergamon Press, Oxford, UK. 1964.
28. T. Suzuki, Y. Yamaguchi, H. Yamamoto, and H. Watanabe. J. Phys. Soc. Jpn. **34**, 911 (1973). doi:10.1143/JPSJ.34.911.
29. Y. Yamaguchi and H. Watanabe. J. Phys. Soc. Jpn. **44**, 1782 (1978). doi:10.1143/JPSJ.44.1782.
30. P. Radhakrishna, H. Fujii, P.J. Brown, S. Doniach, W. Reichardt, and P. Schweiss. J. Phys. Condens. Matter, **2**, 3359 (1990). doi:10.1088/0953-8984/2/14/020.